International Journal of Innovative Computing, Information and Control
Volume **8**, Number **7(B)**, July **2012**

ICIC International ©2012 ISSN 1349-4198
pp. 5121–5136

DEVELOPING A NEW AUTOMATIC VISION DEFECT INSPECTION SYSTEM FOR CURVED SURFACES WITH HIGHLY SPECULAR REFLECTION

Chang Jiang Li[1,2], Zhong Zhang[1], Ippei Nakamura[1], Takashi Imamura[1]
Tetsuo Miyake[1] and Hisanaga Fujiwara[3]

[1]Instrumentation Systems Lab
Toyohashi University of Technology
1-1 Hibarigaoka Tenpaku-cho, Toyohashi 441-8580, Japan
{ li; zhang }@is.pse.tut.ac.jp

[2]Department of Mechanical and Engineering
Chongqing University of Science and Technology
Chongqing University Town, Chongqing 401331, P. R. China

[3]Industrial Technology Center of Okayama Prefecture
5301, Haga, kitaku, Okayama 701-1296, Japan
hisanaga_fujiwara@pref.okayama.lg.jp

Received May 2011; revised September 2011

Abstract. *This paper aims to create an automatic vision defect inspection system that is capable of detecting defects on highly specular reflection curved surfaces, especially for chrome-plated surfaces. These are strongly specular surfaces with very weak diffuse reflection. It is impossible to detect all the defects in one image in which defects may be covered by highlight regions or do not appear because the defects' shapes or positions are random when the object is illuminated. A set of images are captured under different illumination conditions with an optimized relative position and illumination parameter. In the set of images, the specular spots move smoothly on the intact surface and the defects appear randomly as the light source moves. A synthetic image in which specular spots have been removed is reconstructed from the set of images. Moreover, defects are integrated in the synthetic image with higher defect expressivities. Finally, defects can be extracted by combining template matching and morphology techniques. The presented automatic vision defect inspection system has been implemented and tested on a number of simulation images and actual highly specular parts. Encouraging experimental results show that our method is robust, effective and feasible.*
Keywords: Vision defect inspection, Highly specular reflection surface, Image reconstruction, Morphological technique, Template matching

1. **Introduction.** Highly specular surfaces, such as machined surfaces, painted surfaces and plated surfaces are highly reflective, so their inspection is a difficult problem met frequently within the automatic control of industrial parts. Hereafter, we call these surfaces highly specular reflection (HSR) surfaces. The visual inspection of the appearance of metal components in most manufacturing processes mainly depends on human inspectors whose performance is generally subjective, variable, and therefore inadequate. An automatic vision inspection system offers objectivity, better reliability and repeatability and is able to carry out defect measurement to evaluate the industrial part's quality. Kim and Koivo [1], for example, built a system for the automated inspection of wood surfaces. Piironen [2] developed an automated visual inspection system for rolled metal surfaces. Fernandez et al. [3] developed a surface inspection system for casting surfaces,

Rohrmus [4] built a system for web defect detection and Boukouvalas et al. [5] reported an inspection system for ceramic tiled surfaces.

However, methods enabling an automated inspection of the HSR surfaces, in particular HSR curved surfaces, are still lacking. Few papers of HSR surface inspection have been published. A typical kind of vision system has been built to inspect defects on mirror-like objects by analyzing the deformation of lighted stripes [6]. Because of the rather heavy formalism involved in computing defect geometry from the deformation of the lighted stripes, these methods, although accurate, are extremely time-consuming. Another typical system was proposed by setting a novel lighting solution to reveal defects. For instance, Denis Aluze et al. [7] presented a vision system to detect bump defects (e.g., dust and hair) on mirror-like objects. The lighting system was composed of a metallic grid in translation in front of a black light source to obtain a set of images. Pradeep Gnanaprakasam et al. [8] proposed a vision system to detect raised topological defects on smooth specular coatings. This system solved the highlight problem on flat HSR surfaces. However, it was incapable of curved surface inspection because highlights from the curve surfaced, which cannot always be avoided in one image, may mask the true location of the objects and lead to incorrect measurements.

Another challenge for an HSR curved surface is that defects on the HSR curved surface with very weak diffuse reflection are too sensitive to illumination direction to form recognizable information. The reason is that the curved surface topography is complex and defect properties such as shape, direction and location are complex and various. Figure 1 shows two photos of chrome-plated parts, which were taken in a natural environment, and presents the above-mentioned appearance and challenge. The environment surrounding the object can be observed because HSR surfaces of mirror-like objects reflect light-rays directly. In addition, some highlights completely cover some surfaces, so we do not know whether there are defects in these bright regions. Based on the above discussion, we can conclude that not all defects on a surface can be illuminated and form recognizable illuminated spots in one obtained image of a HSR curve surface.

In recent years, for chrome-plated part, the authors [9,10] presented a special random sampling method (SRSM) to separate the specular reflection components and convert the input images into synthetic images that contain only diffuse reflection components. Furthermore, in order to identify defects on HSR surfaces, a template matching method was used in their proposed inspection system. This technique has little computational

(a) Cover-knob (b) Car's brand

FIGURE 1. Examples of HSR curve surfaces

cost and online processing is possible. However, more than twenty images are taken with different light source directions, so this limits its real-world applicability. Furthermore, the template matching technique has the drawback of being sensitive to changes of the relative position and the photographic environment between the inspection part and the template one.

In this study, to address the problems above, we developed a new automatic vision defect inspection system for HSR curved surfaces. The primary significance and novelty of this work is in achieving defect inspection on HSR curved surfacse (e.g., chrome-plated surfaces). The objects in this paper are not only surfaces with highly specular reflection but also circumscribed curve surfaces. This is a significant advancement over the previous method. First, optimal illumination parameters are set to ensure high defect expressivity and considerably less highlight reflection in the inspection region. Second, in order to completely avoid the loss of defects and to solve these challenge which result from various defects on HSR curved surfaces, the proposed system captures several images illuminated under different illumination directions, respectively. Third, a synthetic image is reconstructed from the set of images. In the synthetic image, all defects are integrated with high contrast and bright regions are eliminated. Finally, a novel defect inspection method, which combines the morphological technique and the template matching technique is proposed to correctly identify the kinds of defects from the synthetic image.

Some experiments on HSR curved surfaces such as chrome-plated Acrylonitrile Butadiene Styrene (hereafter referred to as chrome-plated ABS) resin were carried out using our system. The experiments show that this system can reliably detect defects on HSR curved surfaces and that the system is robust to the shape and location of the defect which is extracted in the synthetic image reconstructed from a set of images. Moreover, the inspection system is cost-efficient because of the low algorithmic complexity and is suitable for use in industrial applications.

The remainder of the paper is organized as follows. In the next section, the automatic vision inspection system is introduced and specular reflection processing strategies are shown in Section 3. The defect detection method that combines the morphology technique with template matching is presented in Section 4. And then, Section 5 demonstrates some experiments with HSR curved surfaces and shows good performance of our technique. Finally, in Section 6, we state the conclusions of this paper.

2. **A New Automatic Vision Inspection System.**

A schematic of the automatic surface inspection system prototype is presented in Figure 2. The inspection system consists of acquisition system has a lighting source system and a CCD camera. For the camera we chose the most popular sensor, the charge coupled device. It is popular among industrial users mainly because of its high reliability, shock resistance, high sensitivity, resistance to electromagnetic interference and the linearity of its response with respect to luminance. The CCD camera which provides an 8-bit grey level image was mounted in a fixed position perpendicularly above the work piece.

2.1. **Light source system.**

The choice of a suitable illumination source is crucial to ensure a reliable analysis of the HSR surface. Different objects require different lighting conditions, and different light sources will affect the measurement results. Diffuse illumination, which provides intense uniform light in every direction, can eliminate shadows and greatly reduce the effect of specular reflections. The objects in this paper feature very strong specular reflection with weak diffuse reflection [9,16]. Hence, a diffuse illumination source with a certain direction, that is, side illumination, has been adopted. The illumination position is defined by (θ, φ), as shown in Figure 2, where θ denotes the elevation

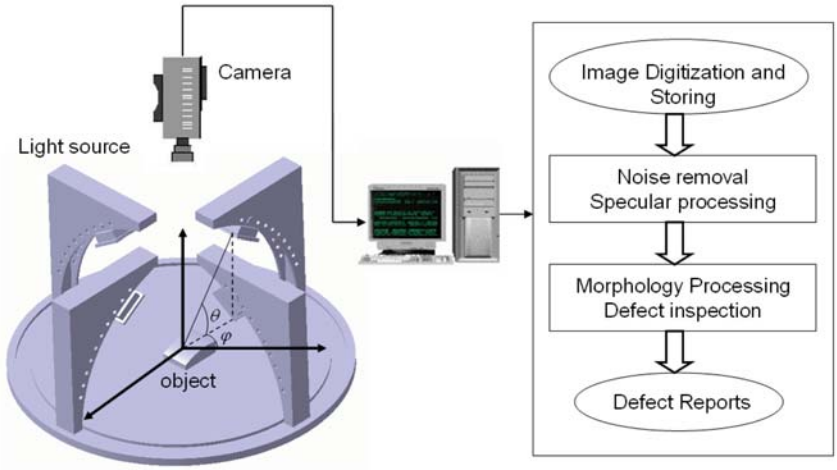

FIGURE 2. The schematic representation of the automatic vision inspection system

angle and φ the azimuth angle. This can reduce specular reflection from the surface and enhance the edge brightness. This is favorable for inspecting objects with highly specular or uneven surfaces. In this inspection system, a square LED with white light and a separate constant current source with intensity control were adopted. Many experiments with the HSR curved surfaces, such as chrome-plated surfaces, show that the defects to be detected are clearer compared with the surrounding region under proper light intensity and incidence direction. However, specular reflection from HSR curved surfaces cannot be completely avoided through the use of a uniform diffuse light source. On the other hand, a variety of defects which have different geometry shapes and locations may not be illuminated or covered by bright regions.

Based on the discussion above we confirm that surface defects cannot be obtained correctly and completely from one image of an HSR surface. So, as shown in Figure 2, an illumination system has been specially designed in the proposed inspection system. A group of light sources are mounted on their rack, respectively. The light source distribution and illumination parameters play an important role in obtaining favorable images. They mainly depend on the topography and optical properties of the object under investigation. Generally, the group of light sources should be evenly separated and of fixed elevation. In Section 5 the optimized illumination system will be discussed further for inspection objects.

2.2. **Measuring environment and defect inspection procedure.** In our application, the inspection system is in a dark room. The object is fixed properly on the work piece. Under certain illumination conditions, the location of the object mainly depends on its surface shape. In the current research, we placed the object to ensure less highlights and distinct highlight regions from different images.

As shown in Figure 2, the defect inspection procedure is performed as follows. First, in the image acquisition stage, four (or more) images are generally captured from the object illuminated by four different incidence directions in turn. Second, the specular processing procedure is performed to remove the specular reflections and enhance the defect expressivity. After this processing, all defects are successfully gathered in a synthetic image reconstructed from the input images. Third, the synthetic image is submitted to the noise removal stage and all defects are extracted by combining template matching and morphology techniques. Finally, the system outputs the detection results and provides information on whether there are any defects on the surface and other analyses.

3. **Multi-image Reconstruction Method for Specular Reflection Processing.** In this section, we introduce the specular reflection processing method of our vision inspection system. Based on reflection analysis of HSR surfaces, a novel method is proposed to process specular reflection from a set of images. Moreover, all defects that may appear in different images were integrated into a single image. In addition, a simulation result is presented to confirm the effectiveness of the proposed method.

3.1. **Relation between reflection and lighting direction.** In the Lambertian Reflection Model (LRM) [13], if both the target object and the viewing position are fixed, the observed image depends only on the lighting direction. Nayar et al. [14] proposed a reflectance framework for smooth and rough metallic surfaces. The model is comprised of three reflection components: the diffuse lobe, the specular lobe, and the specular spike. The diffuse component is represented by the Lambertian model [13]. The Torrance-Sparrow model [15] is used to predict the specular lobe, which depends mainly on the surface properties and the angle between the viewing angle and the normal vector of the point observed. Moreover, the specular lobe component also depends on the direction of the light source and the normal direction of the impinged point. Optical measurement showed that diffuse reflection of the object in this paper was very weak while specular reflection was very strong [16-18].

In order to simulate specular and shadows effects, we produced simulated images using a simple Torrance and Sparrow (T&S) model [15]. Light sources with the same 45° elevation angle θ are equally distributed around the ball. Figure 3 shows specular spots shifting as the light direction changes, where (a) shows the simulation condition of the light direction setting and (b) the simulated images. As shown in Figure 3(b), six images of the non-Lambertian ball and background are generated from the (T&S) model. It will be noted that the shadow and highlight region on the hemisphere changes with different incident angles. This means that by selecting different incident angles, the images with different locations of the shadow and highlight regions can be obtained.

Whenever the macrostructure of the surface under consideration is a spatially slowly varying signal with low-pass characteristics, we will consider it a smooth surface. Due to the smoothness of smooth surfaces, the normal direction will change smoothly and gradually. So, according to the reflection law it is obvious that the specular spot reflected

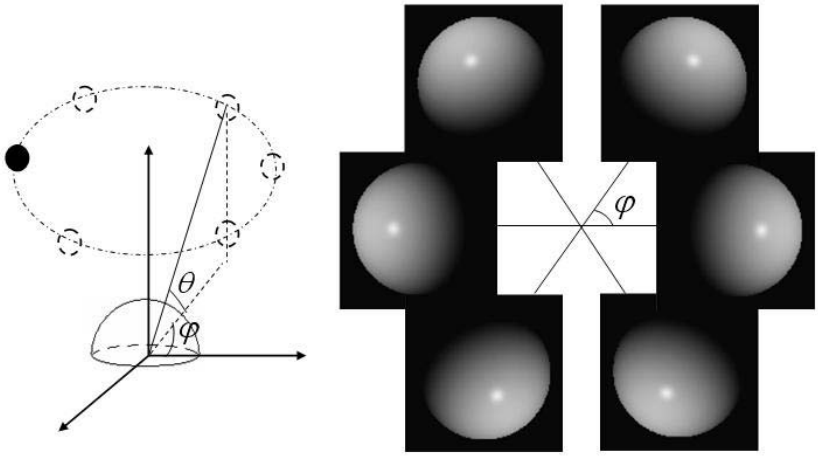

(a) Lights direction setting (b) Six simulated images

FIGURE 3. Specular spots shift as the light direction changes

from the flawless smooth surface will also move smoothly and gradually when the light source smoothly moves.

On the other hand, defects will change the smooth surface normal vector, the detected defects, e.g., a small dot or scratch, and deflect light-ray paths. In Section 5, we will present further discussion with respect to the different reflection between flawless parts and flawed parts on the specular surface.

Based on the above analysis, we develop a multi-image reconstruction method to process specular reflection. This method allows us to reconstruct a synthetic image with free specular reflection on an HSR surface. Moreover, all defects are successfully gathered in a synthetic image reconstructed from the input images.

3.2. **Multi-image reconstruction method for constructing the synthetic image.** In the scope of this paper, a synthetic image is reconstructed from a set of images captured under a fixed viewpoint and different illumination directions. The procedure is as follows. First, a set of images is captured. Second, the intensity gradient of each input image taken with a certain light source direction is calculated. Then the new gradient image from all input images is obtained to eliminate outliers. Finally, we reconstruct a synthetic image from the new gradient data. The synthetic image will be used for further processing, for example, defect inspection.

Let I_k $(1 \leq k \leq n)$ be one of a series of images where I denotes pixel intensity and sub-index k denotes the sequence number of the image taken with light source direction number k. If now a certain pixel (x, y) in all input images on the smooth surface is observed, we can find the course of the gradient variation of the pixel. If the gradient of the pixel (x, y) is the highest among all input images, the pixel is certainly at a specularity boundary. On the other hand, if pixel (x, y) is in a specularity region or in a shadow region, the gradient of the pixel will be close to zero, which is the lowest among all input images. Therefore, we can eliminate the specular pixel by combining the gradient value of the set of images to get a new gradient image. We obtain the new gradient image by the following procedure.

1) Calculate the intensity gradient of every input image that is taken with a certain light source direction.

$$G_k(x, y) = \nabla I_k(x, y) = \begin{bmatrix} \dfrac{\partial I_k}{\partial x} \\ \dfrac{\partial I_k}{\partial y} \end{bmatrix}, \tag{1}$$

where k is the image number $(k = 1, 2 \ldots, n)$, and ∇ is the gradient operator.

2) Get a new gradient image by weighted summation of the intensity gradient at the corresponding position in all input images, that is:

$$G(x, y) = \sum_k \lambda_k G_k(x, y) = \begin{bmatrix} G_x \\ G_y \end{bmatrix}, \tag{2}$$

where λ_k is the weight of the image k, G_x, G_y denotes the median gradient in directions x and y, respectively.

Some methods of deciding an optimal combination of series gradient images have been adopted based on statistical analysis. In this paper, we select a simple method to get the new gradient image. The method is to find the median gradient value at the corresponding position in all of the input images. It is obvious that in the new gradient field, these outliers have been removed and only the gradient values of diffuse reflection components are present. It needs to be noted that the intensity of a pixel resulting from a defect part of the specular reflection surface, which is similar to a specular component, is due to the

sharp change in its normal direction. In addition, these highlights result from a defect present in the same place in most of the series' images although the size of a specular spot may differ slightly. It is evident that the processing method can remove specular reflection components because of the intact smooth surface, but results in the preservation of defect information.

We need to reconstruct the synthetic image using the new gradient value obtained in the above process for future processing. One first assumes the synthetic image $\tilde{I}$ satisfies the equation:

$$\nabla \tilde{I} = G(x, y), \tag{3}$$

According to the variation principle, the image $\tilde{I}$ that minimizes the integral value in Equation (3) must satisfy the Euler-Lagrange equation:

$$\frac{\partial F}{\partial \tilde{I}} - \frac{d}{dx}\frac{\partial F}{\partial \tilde{I}x} - \frac{d}{dy}\frac{\partial F}{\partial \tilde{I}y} = 0. \tag{4}$$

Then, we can get the Poisson equation:

$$\nabla^2 \tilde{I} = divG, \tag{5}$$

where $\nabla^2 \tilde{I} = \frac{\partial^2 \tilde{I}}{\partial x^2} + \frac{\partial^2 \tilde{I}}{\partial y^2}$, ∇^2 is the Laplacian operator and $divG = \frac{\partial G_x}{\partial x} + \frac{\partial G_y}{\partial y}$ is the divergence of the new gradient values G. For a 2-D digital image, we use the DCT method to solve Equation (5) and get the synthetic image $\tilde{I}$.

The approach is based on the premise that specular reflection should move gradually when the light source that illuminates the object moves. It is worth noting that in the group of images the specular reflection and shadow cannot overlap completely. So, in our method, four images are captured evenly apart and of fixed elevation. In general, four images of a considerably complex curvature surface can reveal the whole surface's information even though the object is not ideally diffuse. In fact, for an ideal diffuse surface, three images are enough. Fortunately, smooth and highly specular surfaces are very sensitive to changes in the light sources. On the other hand, a large number of images are not necessary for considerably complex curvature surfaces. Of course, for those very complicated surfaces more than four images may be needed. On the other hand, a large number of images will make that specular region overlap in several images. A large number of experiments for our objects show that four images are enough for defect inspection of a smooth, highly specular surface.

3.3. **Specular processing results obtained from the model image.** Figure 4 shows a simulation result, where the object is a vase. We rendered four images by the reflection model [14] and the vase surface shape 3D data, where the illumination elevation angle was fixed at 60° and their azimuth angles were 30°, 120°, 210°, 300° from left to right, respectively. The fifth image shown in Figure 4(e) is the synthetic image. Figure 5(a) shows an example of the histogram of the original image shown in Figure 4(a) and Figure 4(b) shows the synthetic image. From Figure 5(a) we can observe that there are many highlight reflections, while the synthetic image shown in Figure 4(d) shows there are few or no pixels with high intensity values because the specular reflection components are significantly removed by the above proposed method. On the other hand, the histogram of the original image is a non-normal distribution which shows the brightness distribution is partially bright, dark or of excessively concentrated brightness. The histogram of the synthetic image follows the normal distribution, which indicates the synthetic image is favorable to further processing.

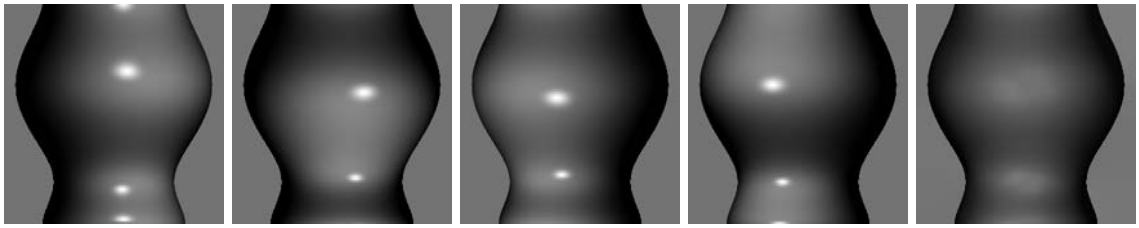

(a) 30° (b) 120° (c) 210° (d) 300° (e) synthetic image

FIGURE 4. Specular processing for a rendering surface change, where the illumination elevation angle θ is fixed at 60° and the azimuth angles φ are 30°, 120°, 210°, 300° from left to right, respectively

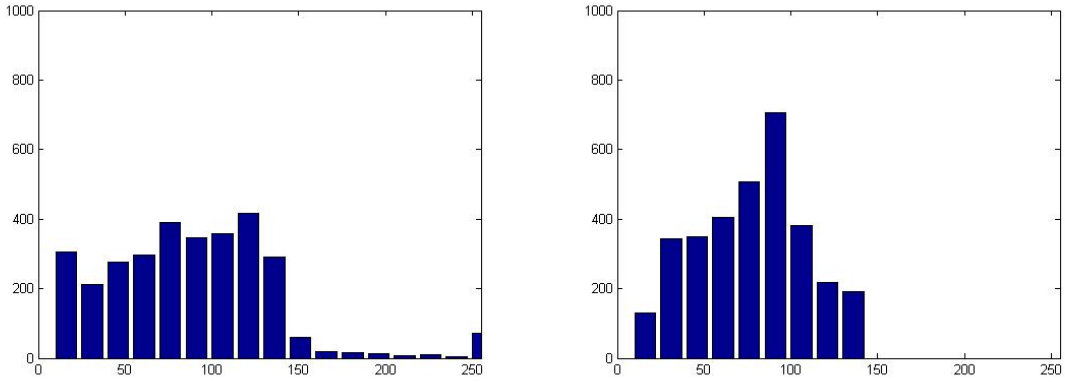

(a) Histogram of the original image (b) Histogram of the synthetic image

FIGURE 5. Histograms of the original and synthetic images

3.4. **Specular processing results obtained from real HSR curved surfaces.** The object to be confirmed is a car doorknob, which is an electroplating surface. Some simulated defects are made over the object, whereas defects are placed in several positions. In order to test the processing method under different situations, those defects were of different sizes, shapes and major directions.

Figure 6 shows four gray images of size 600 × 400 [pixel], which were obtained in the condition of the illumination elevation angle θ being fixed at 60° and the azimuth angles φ being (a) 0°, (b) 180°, (c) 225°, (d) 315°, respectively. The azimuth angles were set especially according to the topography of the surface under investigation (the details of the setting method will be presented in Section 5.1). As shown in Figure 6, first, big bright regions occur with different positions in the four images, and this is consistent with the above reflection analysis previously mentioned. Second, some defects in the original images are either covered by a bright region or present low contrast. So, it is almost impossible to perceive all defects in any one image of the four images. Figure 7 shows the synthetic image that was reconstructed from the images shown in Figure 6 by using proposed method and the defects are marked by rectangles. To evaluate the performance of the specular processing, we compared the image with the original images in Figure 6. For example, as shown in Figure 6(b), the three left-most defects are covered by a bright region. Similarly, the right-most defects are covered by the bright region in Figure 6(a). However, they have been completely recovered in the synthetic image. Moreover,

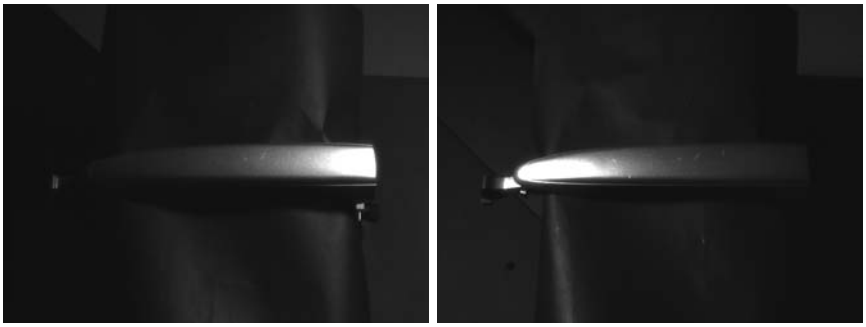

(a) 0° (b) 180°

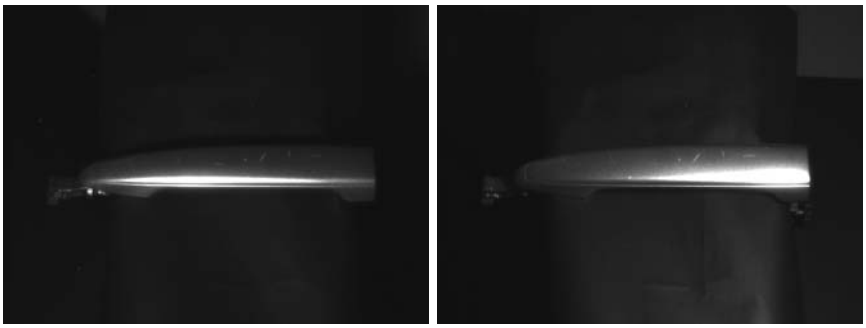

(c) 225° (d) 315°

FIGURE 6. Four original images of a car doorknob with defects, where the illumination elevation angle is fixed at 60° and the azimuth angle is (a) 0°, (b) 180°, (c) 225°, (d) 315° respectively

FIGURE 7. The synthetic image reconstructed from Figure 6

thanks to the reconstruction approach, all defects have been gathered simultaneously in the synthetic image. Therefore, we can conclude that our method is effective for removing specular reflection and saving useful surface information of defects at the same time. In this paper, we will inspect correctly all defects on smooth specular reflection surfaces from the synthetic image.

4. **A New Defect Detection Method.** After specular processing, we obtain the object surface image with free specular reflection components. So the main objective of this section is to extract defects from the synthetic image. The conventional template matching technique is to subtract the sample image from the template image according to gray level. It is sensitive to noise and misalignment between the two images. On the other hand, in our application a little specular reflection in such locations as edges and cross points also

affects the result from the traditional approach method. We show a new defect detection method, which combines the morphology technique with template matching that can overcome the shortcomings of the traditional method.

4.1. **Review of morphology operations and defect detection algorithms.** The morphological operation is one of a number of operations consisting of combinations of the Minkowski sum and Minkowski difference of two sets A and B, which can be shown in Equations (6) and (7), respectively [17]. In the case of image processing, the set A is called the target element and set B is the structural element.

$$A \oplus B = \{z \in E\colon\ z = a + b, a \in A, b \in B\} \tag{6}$$

$$A \ominus B = \left\{z \in E\colon\ x - b \in A, b^{\forall} \in B\right\} \tag{7}$$

Generally, the Minkowski sum calculation is called Dilation and the Minkowski difference calculation is called Erosion. Furthermore, performing Dilation after Erosion is called Opening and performing Dilation before Erosion is called Closing. Figure 8 shows an example of the morphological operations in the case of a binary image. As is shown in Figure 8, Dilation causes the target figure to expand and Erosion causes the target figure to shrink. Opening removes only the convexities and isolated regions of the target figure, and Closing removes only concavities and holes.

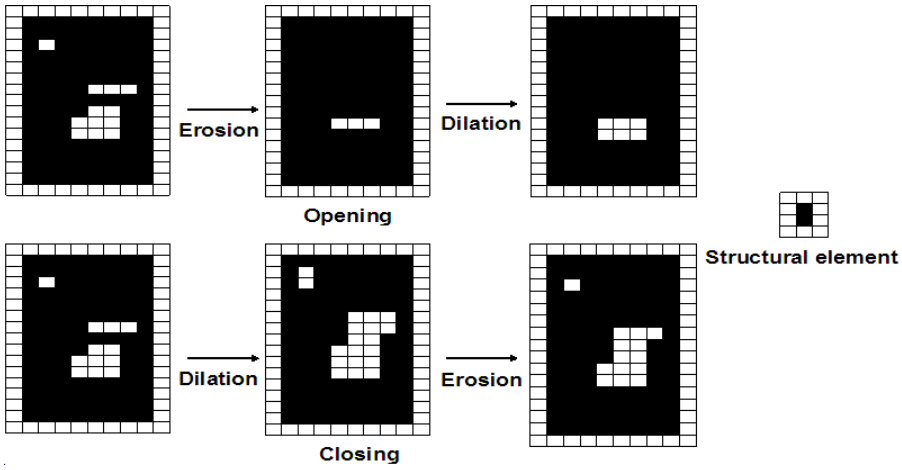

FIGURE 8. Example of the morphological operation applied to a binary image

Assume a grayscale image has horizontal axis x, vertical axis y, and let the brightness be represented by $f(x, y)$. In one dimension, such as along the x axis, the Dilation operation can be shown as Equation (8) and the Erosion operation can be shown as Equation (9).

$$(f \oplus g)(x) = \max_{\substack{x-z \in F \\ z \in K}} \{f(x - z) + k(z)\} \tag{8}$$

$$(f \ominus g)(x) = \min_{\substack{x+z \in F \\ z \in K}} \{f(x + z) - k(z)\} \tag{9}$$

where $f(x)$ denotes the original image, $k(z)$ is the structural element, and F and K show the domain of the structural element.

Figure 9 shows an example of the morphological operation for a grayscale image, where (a) shows $f(x)$, (b) shows the structural element $k(z)$, (c) shows the result obtained from Equation (8) and (d) shows the result obtained from Equation (9). As is shown in Figure 9, in the case of the Dilation operation, pixels whose intensity values are much higher than those of neighboring pixels and whose area is smaller than the structural element

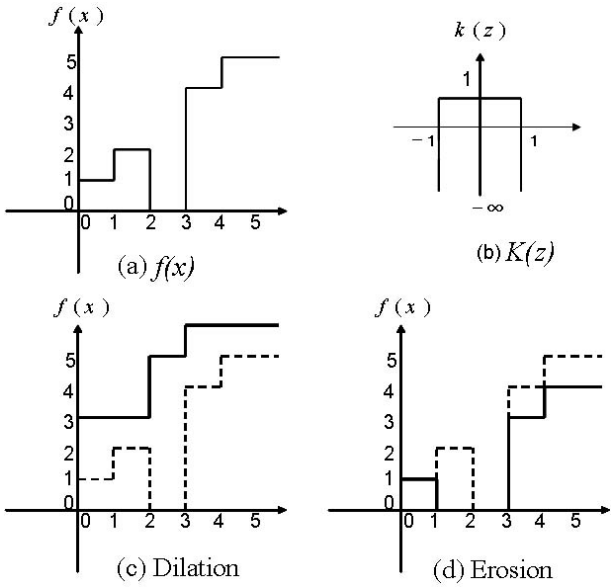

FIGURE 9. Example of the morphological operation for a grayscale image

are removed. Contrarily in the case of the Erosion operation, pixels whose values are much lower than those of neighboring values and whose area is smaller than the structural element are removed.

4.2. **Defect detection algorithms.** Figure 10 shows the defect inspection procedure proposed in this paper. In the first step, we perform the opening operation, difference, and image segment operation. And then, the image obtained in the above operation is converted to a binary image by using a suitable threshold. We set the binary image of the object under investigation as bwI_s. In the same way, we construct the template image from the flawless surface and set it as bwI_t.

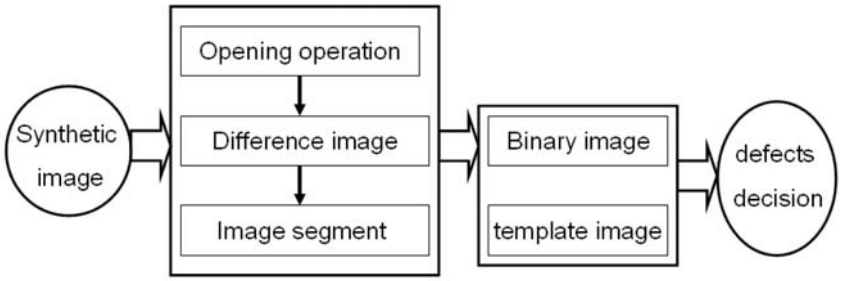

FIGURE 10. The defect inspection procedure from the synthetic image

Lastly, we detect defects by subtracting the template binary image bwI_t from the sample binary image bwI_s according to Equation (10).

$$D(i,j) = bwI_s(i,j) - bwI_t(i,j) \tag{10}$$

where $D(i,j)$ represents the difference between bwI_s and bwI_t. We consider any pixel whose value is one as being in a defect. We have to fill some holes in the resultant binary image $D(i,j)$ to make a close region and eliminate the noise. On the other hand, we classify those regions whose areas are larger than a set threshold as belonging to defects.

In addition, we need to dilate the template binary image bwI_t before performing the subtract calculation. This operation can guarantee that the edge of the template is wider

than in the sample image. Moreover, when there is a small difference in location between the sample and template, the approach is also robust. That is, in this way, the drawback of template matching being sensitive to changes in the relative position of the inspection part and the template, and being sensitive to changes in the photographic environment can be overcome.

5. **Experimental Results and Discussion.** This section presents some confirmation experiments. These inspected surfaces are HSR curved surfaces, which are broadly found in the automotive industry because of their bright appearance.

5.1. **Illumination elevation angle setting.** A diffuse light source can illuminate an object uniformly. But for a chrome-plated, HSR surface with a complex curve, it is very important to set the illumination location to guarantee less specular reflection. This mainly depends on the macro surface shape of the object to be detected. Moreover, this also depends on the microscopic shape of those defects. However, defects are random in regards to shape, major axis direction, size and location. So, based on the discussion in Section 3.1 we experimentally set the illumination configuration, which consists of the elevation angle θ and the azimuth angles φ.

In order to numerically evaluate the optimal lighting configurations, the defect expressivity σ is defined by the following formulas. The mean intensity of the region of interest is:

$$M = \sum_{i=0}^{255} \left(i \times \frac{n_i}{N} \right). \tag{11}$$

The mean intensity of the defect region is:

$$M' = \sum_{i=0}^{255} \left(i \times \frac{n_i}{N'} \right). \tag{12}$$

The defect expressivity σ is

$$\sigma = \frac{M - M'}{M}, \tag{13}$$

where n_i is the number of pixels whose intensity is i, N and N' are the total numbers of the regions of interest and defect regions, respectively.

The bigger the defect expressivity σ, the more easily defects can be detected. The defect expressivity depends not only on the defect shape type and orientation but also the illumination direction and intensity.

5.2. **Inspection on HSR curved surfaces.** In order to test the performance of the proposed inspection system, many experiments have been performed. In this section, we present two examples of these experiments. The first object is the cover-knob covered with chrome-plated ABS resin [9], which is one of the shiniest specular reflection surfaces. The other object was tested on a car door-knob.

The first object under investigation is a car cover-knob, on which two defects have been confirmed by the inspectors. Their sizes are of 1.0×0.8 [mm] and 0.8×0.4 [mm], respectively. Figure 11 shows four original gray images of size 600×400 [pixel] captured from the object illuminated by four different directions in turn, and the illumination elevation angle θ is set at 60° and the azimuth angles φ are set at (a) 30°, (b) 120°, (c) 210°, (d) 300° by Equations (11), (12) and (13), respectively. And the resolution of the inspection system is set at 0.075 [mm/pixel] according to the inspection standard and morphology technique. For the sake of the next illustration, we call the defect marked by the circle defect A and the defect marked by the rectangle defect B. Defects A and B

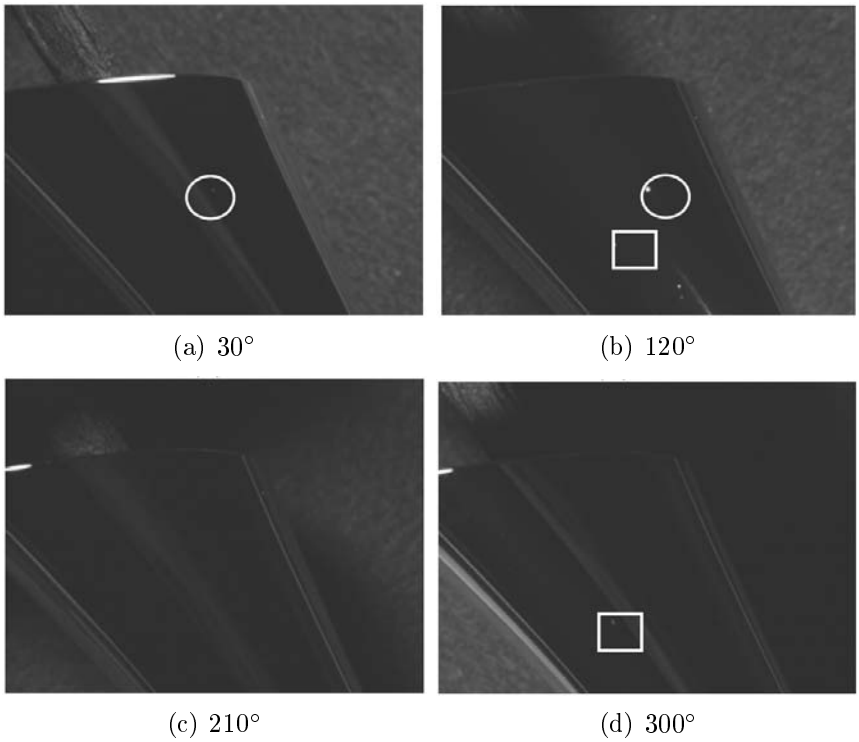

(a) 30° (b) 120°

(c) 210° (d) 300°

FIGURE 11. Four original images of the chrome-plated ABS resin taken with different illumination directions, where the illumination elevation angle is fixed at 60° and the azimuth angle is (a) 30°, (b) 120°, (c) 210°, (d) 300° respectively

are of different shapes; A is a small dot and B is a thin scratch. First, in each original image shown in Figure 11, most of the pixels are very dark, whose intensities are close to 0. It can be confirmed that the illumination system successfully avoids specular reflection from a flawless surface. So, we can indicate that the lighting system with side and diffuse illumination succeeds in reducing the specular reflection from a smooth surface, although some brightness appears at the edge. Second, it is obvious that their reflections strongly depend on the illumination direction, so we cannot find all defects from any one image. From the above discussion, we can say that all defects could be detected only from multiple images captured with different directions.

Figure 12 shows the processed results by the proposed method, where (a) denotes the synthetic image reconstructed from the four images shown in Figure 11 and (b) the morphology processing result of (a). To evaluate the specular processing, we compared the synthetic image with the original images of Figure 11. For example, as shown in Figure 11(a), only defect A appears with very low contrast, and the worst case is that defect B does not appear. And a highlight band appears on the top edge. In particular, all defects cannot be found in Figure 11(c). In contrast, in the synthetic image the highlight band was completely removed and the two defects simultaneously appear with considerably high contrast. On the other hand, in the center of the synthetic image some uneven intensity can be found, which will make the next defect inspection difficult or erroneous. So we use the morphology operation to eliminate this phenomenon. Figure 12(b) shows the morphology operation result and the improvement can be confirmed.

Figure 13 shows defects detection results by the proposed method, where (a) shows the binary image of the sample part, (b) shows the binary image of the template part,

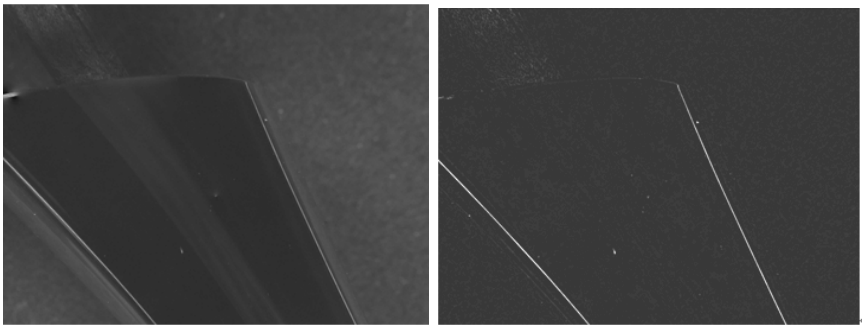

(a) Synthetic image (b) After morphology processing

FIGURE 12. Morphology processing result, where (a) is the synthetic image and (b) is the image after morphology processing

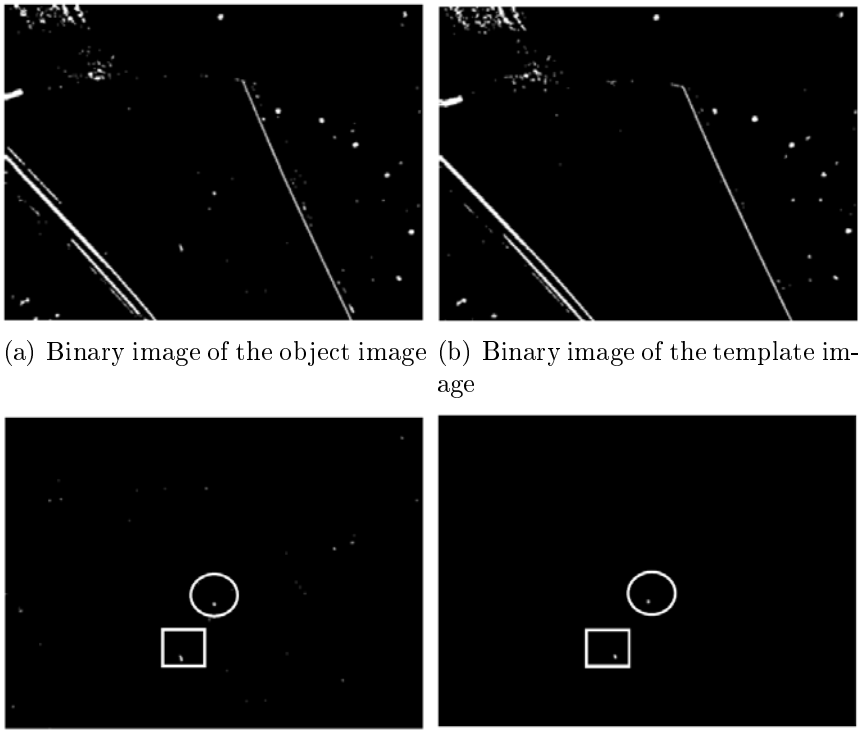

(a) Binary image of the object image (b) Binary image of the template image

(c) Result of template matching (d) All defects

FIGURE 13. (a) Defect inspection results obtained by combining morphology processing and template matching, where (a) shows the binary image of the object image, (b) the binary image of the template image, (c) the result of template matching and (d) all defects

(c) shows the result of template matching obtained by subtracting the target image from the template image, and (d) shows the final result after noise removal. In order to guarantee the effectiveness of the proposed method, we have to dilate the template image to enlarge the edge size. This means that when the target and the sample are slightly out of alignment, our method is still effective. Furthermore, the car manufacturer set a manufacturing standard such that objects with defect sizes of more than 0.25 [mm] are to be rejected. According to the standard and system resolution of 0.075 [mm/pixel],

we remove those small white spot noise by the erosion algorithm using a 3×3 square structure element and detect the two defects.

In the second object, the car doorknob shown in Figures 6 and 7, whose size is of 180×40 [mm], has been inspected using the proposed inspect system. Among the defects marked by the rectangle shown in Figure 7, two defects are dots, and the others are scratches, whose appearance is thin and long. Their sizes are from 0.25 [mm] to 4.2 [mm]. In particular, these scratch defects with various orientations exist on different locations on the surface. Figure 14 shows defect inspection results obtained from Figure 7 by using the proposed method. The inspection result is consistent with the manual inspection result. Furthermore, the other experiments also obtained nice results. Therefore we can conclude that this inspection system can reliably detect defects on HSR curved surfaces and it is robust to the shape and location of the defects.

FIGURE 14. Defects inspection result of the car doorknob

6. **Conclusion and Remarks.** In this paper, we proposed a new automatic vision defect inspection system, which focuses on detecting defects on HSR curved surfaces, especially for chrome-plated surfaces. The results obtained can be summarized as follows:

1) A new multi-image reconstruction method has been proposed for specular processing by reconstructing a synthetic image from a set of images, which were taken with different light directions. Simulation and experiments demonstrate that it successfully gathers all defects and eliminates specular regions.

2) The lighting system with side and diffuse illumination was selected for our inspection system and it succeeded in reducing the specular reflection from a smooth surface, although some brightness appeared at the edge.

3) A novel defect inspection method, which combines the morphological technique with template matching, was proposed to correctly identify the kinds of defects from the synthetic image. It is very cost-efficient because of the low algorithmic complexity and can match the needs of the production line.

4) The proposed automatic vision defect inspection system, which consists of three components (image acquisition, specular processing, and defect inspection), has been tested on many HSR curved surfaces with various defects. Experiments show that this system can reliably detect defects on HSR curved surfaces and it is robust to the shape and location of the defects.

In the future, we would like to focus on increasing the performance of this inspection system and implement the inspection system on the production line. However, deriving the optimal illumination system from the surface topography and reflection properties of the surface under investigation is the next work to be done. Segmenting the 3D surface [19]

into several different regions according to surface curvature and setting the corresponding light direction would make this system high performance.

Acknowledgment. This work was supported by the Global COE Program "Frontiers of Intelligent Sensing" from the Ministry of Education, Culture, Sports, Science and Technology, Japan. Test samples were supported by Vienna University of Technology.

REFERENCES

[1] M. Nitta, An image processing technology trend in metal surface inspection, *Journal of Denki-Seiko*, vol.149, no.5, pp.379-386, 2002.

[2] D. Rohrmus, Invariant texture features for web defect detection and classification, *SPIE Proc. of Machine Vision Systems for Inspection and Metrology VIII*, Boston, MA, vol.3836, pp.144-155, 1999.

[3] C. Boukouvalas, J. Kittler, R. Marik and M. Petrou, Automatic grading of ceramic tiles using machine vision, *Proc. of the IEEE International Symposium on Industrial Electronics*, pp.13-18, 1994.

[4] B. Denkena, H. Ahlers, F. Berg and T. Wolf, Fast inspection of larger sized curved surfaces by stripe projection, *Annals of CIRP*, vol.51, no.1, pp.499-502, 2002.

[5] D. Perard and J. Beyerer, Three-dimensional measurement of free-form surfaces with a structured-lighting reflection technique, *SPIE Conference on Machine Vision Application in Industrial Inspection, Pittsburgh (USA)*, vol.3204, pp.74-80, 1997.

[6] S. K. Nayar, A. C. Sanderson, L. E. Weiss and D. A. Simon, Specular surface inspection using structured highlight and Gaussian images, *IEEE Transactions on Robotics and Automation*, vol.6, no.2, pp.208-218, 1990.

[7] P. Gnanaprakasam, J. M. Parker, S. Ganapathiraman and Z. Hou, Efficient 3D characterization of raised topological defects in smooth specular coatings, *Image and Vision Computing*, vol.27, pp.319-330, 2009.

[8] D. Aluze, F. Merienne, C. Dumont and P. Gorria, Vision system for defect imaging, detection, and characterization on a specular surface of a 3D object, *Image and Vision Computing*, vol.20, pp.569-580, 2002.

[9] Z. Zhang, S. Ren, T. Miyaki, H. Fujiwara and T. Imamura, Processing reflections on metallic surfaces using a special random sampling method, *International Journal of Innovative Computing, Information and Control*, vol.4, no.7, pp.1595-1606, 2008.

[10] S. Q. Ren, Z. Zhang, T. Miyake, H. Fujiwara and T. Imamura, Edge detection of highly specular surface using special random sampling method, *Proc. of the 4th International Conference on Innovative Computing, Information and Control*, Kaohsiung, 2009.

[11] M. Nitta, An image processing technology trend in metal surface inspection, *Journal of Denki-Seiko*, vol.149, no.5, pp.379-386, 2002.

[12] S. Kojima and T. Miyakawa, 1-dimensional processing architecture for gray-scale morphology, *IEICE TRANSACTIONS on Information and Systems*, vol.J79-D-2, no.1, pp.53-60, 1996.

[13] A. Shashua, *Geometry and Photometry in 3D Visual Recognition*, Ph.D. Thesis, MIT, 1992.

[14] S. K. Nayar, K. Ikeuchi and T. Kanade, Surface reflection: Physical and geometrical perspectives, *IEEE Trans. on Pattern Analysis and Machine Intelligence*, vol.13, no.7, pp.611-634, 1991.

[15] K. E. Torrance and E. M. Sparrow, Theory for off-specular reflection from roughened surfaces, *Journal of the Optical Society of America*, vol.57, no.9, pp.1105-1114, 1967.

[16] A. Ngan, F. Durand and W. Matusik, Experimental analysis of BRDF models, *Eurographics Symposium on Rendering*, 2005.

[17] Z. Zhang, I. Nakamura, C. J. Li, T. Imamura, T. Miyake and H. Fujiwara, Metal plating surface defect detection by template matching using morphological processing, *ICIC Express Letters, Part B: Applications*, vol.2, no.3, pp.615-620, 2011.

[18] N. Araki, K. Nishiuchi, T. Sato, Y. Konishi, E. Fujiwara and H. Ishigaki, Defect detection for mirror polished metal surface using independent component analysis, *ICIC Express Letters*, vol.5, no.9(B), pp.3291-3296, 2011.

[19] I. Yamazaki, V. Natarajan, Z. Bai and B. Hamann, Segmenting point-sampled surfaces, *The Visual Computer*, vol.26, pp.1421-1433, 2010.